Cubosomes for in vivo fluorescence lifetime imaging

Cubosomes for *in vivo* fluorescence lifetime imaging

Stefania Biffi,[a,] Laura Andolfi,[b] Claudia Caltagirone,[c] Chiara Garrovo,[a] Angela M. Falchi,[d] Vito Lippolis,[c] Andrea Lorenzon,[e] Paolo Macor,[f] Valeria Meli,[c] Maura Monduzzi,[c] Marc Obiols-Rabasa,[g] Luca Petrizza,[h] Luca Prodi,[h] Antonella Rosa,[d] Judith Schmidt,[i] Yeshayahu Talmon,[i] Sergio Murgia[c]**

[a]Institute for Maternal and Child Health – IRCCS "Burlo Garofolo", Trieste, Italy.

[b]IOM-CNR, Area Science Park, Basovizza, Trieste, Italy;

[c]Department of Chemical and Geological Science, University of Cagliari, and CSGI, I-09042 Monserrato (CA), Italy;

[d]Department of Biomedical Science, University of Cagliari, I-09042 Monserrato (CA), Italy;

[e]Animal Care Unit, Cluster in Biomedicine (CBM scrl), Trieste, Italy;

[f]Department of Life Sciences, University of Trieste, Italy;

[g]Division of Physical Chemistry, Department of Chemistry, Lund University Getingevägen 60, SE-22240 Lund, Sweden;

[h]Department of Chemistry "G. Ciamician", University of Bologna, Bologna, Italy;

[i]Department of Chemical Engineering, Technion – Israel Institute of Technology, Haifa 3200003, Israel.

Corresponding Authors: stefania.biffi@burlo.trieste.it (SB) and murgias@unica.it (SM)

Abstract

Herein we provided the first proof-of-principle for *in vivo* fluorescence optical imaging application using monoolein-based cubosomes in a healthy mouse animal model. This formulation, administred at a non cytotoxic concentration, was capable of providing both exogenous contrast for NIR fluorescence imaging with very high efficiency and chemospecific information upon lifetime analysis. Time-resolved measurements of fluorescence after the intravenous injection of cubosomes revealed that the dye rapidly accumulates mainly in the liver, while lifetimes profiles obtained *in vivo* allowed discriminating between the dye free or embedded within the cubosome nanostructure after injection.

Keywords: Liquid crystalline nanoparticles, fluorescence lifetime probe, fluorescence optical imaging in vivo.

1. Introduction

Spontaneous self-assembly of lipids in water allows formulation of liquid crystalline nanoparticles of the inverted type, showing inner nanostructure characterized by lipid bilayers wrapped on triply periodic minimal surfaces of cubic symmetry [1–4], a beautiful three-dimensional organization now completely disclosed by cryo-electron tomography [5]. Discovered in the eighties, such nanoparticles are universally known as cubosomes [6,7]. They are considered an emerging platform for a wide range of nanomedicine applications by virtue of unique features [8]. These include a high hydrophobic volume (higher than liposomes) [9], the possibility of simultaneously host both diagnostic agents and therapeutics (cubosomes are also proposed as theranostic tools) [9–11], storage stability, and a viscosity of the formulation close to water, a fundamental characteristic for bolus delivery [12]. Recently, they were successfully tested as carriers for antimicrobial peptides [13], and their superior efficacy in the siRNA delivery (cuboplexes) with respect to traditional lipoplexes was also demonstrated [14]. The necessary colloidal stability of cubosome formulations is typically achieved by using polyethylene oxide (PEO)-polypropylene oxide (PPO)-polyethylene oxide triblock copolymers (Pluronics) as stabilizing agents, although other kinds of stabilizers have been proposed [14–18]. As a consequence, cubosomes are surrounded by a PEO corona that, similarly to stealth liposomes, should retard the clearance from the bloodstream of these nanoparticles via the mononuclear phagocytic system by inhibiting opsonization [19,20]. Furthermore, their surface can be decorated with targeting residues to properly address cubosomes towards specific tissues [21,22]. Despite their remarkable potential as nanocarriers, to the best of our knowledge, so far, no papers have appeared describing the successful exploitation of cubosomes for *in vivo* imaging. Differently, several authors demonstrated that the hexagonal counterpart of cubosomes (namely, hexosomes) can be effectively labeled with radiotracers (such as

^{99}Tc) [23,24] or MRI contrast agents (paramagnetic nitroxide lipids) [12,25], providing valuable imaging tools for *in vivo* diagnostics. Compared with traditional structural and functional imaging modalities, fluorescence optical imaging (FOI) offers several advantages, requiring a relatively simple instrumental setup, and showing high signal-to-noise ratios *in vivo*, owing to the development of novel synthetic fluorescent probes with high brightness and photostability in the near infra-red spectral region (NIR, 650-900 nm) [26–29]. Therefore, innovative FOI methods hold promise as radiation-free, portable, and potentially cost-effective screening technology extremely useful in imaging studies *in vivo* [30]. In particular, Time-Domain optical imaging (TD-OI) technology allows for NIR fluorescence lifetime analysis, which is based both on the specificity of fluorescence probes and the sensitivity of their emission lifetime, related to environmental characteristics [31–36]. In this context, here we provide the first proof-of-principle for FOI application using monoolein (MO)-based cubosomes *in vivo* in a healthy mouse animal model.

2. Materials and methods

2.1. Cubosomes preparation and characterization

Cubosomes were prepared by dispersing melted monoolein (MO, 1-monooleoylglycerol, 98.1 wt%, kindly provided by Danisco A/S, DK-7200, Grinsted, Denmark) in an aqueous solution of Pluronic F108 (PF108, PEO_{132}–PPO_{50}–PEO_{132}, Sigma-Aldrich) using an ultrasonic processor UP100H by Dr. Hielscher, cycle 0.9, amplitude 90%, for 10 min. To obtain fluorescent cubosomes, the fluorophore Cy5.5-C_{14} was dispersed in the melted MO with the help of an ultrasonic bath before dispersion in Pluronic F108. Typical volume of the sample was 4 mL with 96.4 wt % of water, 3.3 wt % of MO, and 0.3 wt % of Pluronic F108. After loading, cubosome dispersion was purified from the non-encapsulated dye by dialysis as

follows: 2 mL were loaded into dialysis tubing cellulose membrane (14 kDa MW cutoff, purchased from Sigma-Aldrich) and dialyzed against water (1000 mL) for 2 h (by replacing the water after 1 h). Loading efficiency (E%), expressed as percentage of the amount of the dye present in the formulation before dialysis, was determined by UV- Vis spectroscopy after disruption of cubosomes (dialyzed and not dialyzed) with acetonitrile. Cy5.5-C_{14} content was quantified before and after purification by a Thermo Nicolet Evolution 300 UV-VIS spectrophotometer at 679 nm. The molar concentration of Cy5.5-C_{14} in the cubosomes sample after dialysis was 2.7×10^{-4}, with E% = 75. Dynamic light scattering (DLS) measurements for the determination of the nanoparticles size and ζ-potential were performed at 25 °C using a ZetaSizer Nano ZSP (Malvern Instruments Ltd., Worcestershire, U.K.). DLS measurements were also performed after the cubosome formulation was passed through a 30G needle (the same used for cubosome i.v. administration for *in vivo* tests), to confirm that injection did not alter the physicochemical characteristics of the formulation. Characterization of the nanoparticles internal structure at 25 °C was carried out by small angle x-ray scattering (SAXS) using a Ganesha 300XL (SAXSLAB ApS, Skovlunde, Denmark). The lattice parameter a of the cubic phases was determined using the relation $a = d(h^2 + k^2 + l^2)^{1/2}$ from linear fits of the plots of $1/d$ versus $(h^2 + k^2 + l^2)^{1/2}$, where $d = 2\pi/q$ (q is the measured peak position) and h, k, and l are the Miller indices. The a value reported is the average (± SD) value calculated from the five Bragg peaks discernible in the diffractogram (see figure 1b). The morphology of the nanoparticles was observed at 120 kV acceleration voltage in an FEI Tecnai T12 G^2 transmission electron microscope at about −175 °C in the low-dose imaging mode to minimize electron-beam radiation-damage. Images were digitally recorded with a Gatan US1000 high-resolution CCD camera.

2.2. Photophysical measurements

Cubosomes solutions were diluted with Milli-Q® water. UV-vis absorption spectra were recorded at 25 °C by means of a Perkin-Elmer Lambda 45 spectrophotometer. Quartz cuvettes with optical path length of 1 cm were used. Corrected fluorescence emission and excitation spectra (450 W, Xe lamp) were obtained with a modular UV-vis-NIR spectrofluorimeter (Edinburgh Instruments FLS920) equipped with both a Hamamatsu R928P photomultiplier tube (for the 500-850 nm spectral range) and an Edinburgh Instruments Ge detector (for the 800-1600 nm spectral range). Luminescence quantum yields (uncertainty ± 15%) were recorded on air-equilibrated solutions and cyanine IR-125 (from Acros Organics) in Ethanol ($\Phi = 0.132$) [37]. The same instrument connected to a PCS900 PC card was used for the TCSPC (Time-Correlated Single Photon Counting) experiments (excitation laser λ = 640 nm). Corrections for instrumental response, inner filter effects and phototube sensitivity were performed [38]. Fluorescence anisotropy measurements were performed on an Edinburgh FLS920 equipped with Glan-Thompson polarizers. Anisotropy measurements were collected using an L-format configuration, and data were corrected for polarization bias using the G-factor. Four different spectra were acquired for each sample combining different orientation of the excitation and emission polarizers: I_{VV}, I_{VH}, I_{HH}, I_{HV} (where V stands for vertical and H for horizontal; the first subscript refers to the excitation polarizer and the second subscript refers to the emission one). Spectra were used to calculate the G-factor and the anisotropy *r*: $G = I_{HV}/I_{HH}$, $r = (I_{VV} - GI_{VH})/(I_{VV} + 2GI_{VH})$. Calculated G value was 1.85.

2.3. Cytotoxicity experiments

Mouse 3T3 fibroblasts (ATCC collection) were grown at 37 °C in phenol red-free Dulbecco's modified Eagle's medium (DMEM, Invitrogen, USA) with high glucose, supplemented with 10% (v/v) fetal bovine serum, penicillin (100 U mL^{-1}), and streptomycin (100 µg mL^{-1}) (Invitrogen) in a 5% CO_2 incubator at 37 °C. The cytotoxic effect of the nanoparticle

formulation was evaluated in 3T3 fibroblasts by the MTT assay [39]. 3T3 cells were seeded in 96-well plates at a density of 2×10^3 cells/well in 100 μL of serum-containing media. Experiments were carried out two days after seeding, when cells had reached 70% confluence. Cubosomes were added to the cells at different concentrations (corresponding to 20, 30, 40, 55, 83, and 165 μg/mL of MO) in 100 μL of serum-free medium, and incubated at 37 °C for 4 h. The cell culture medium was then removed from each well of the 96-well plates; an 8 μL portion of MTT solution (3-(4,5-dimethylthiazol-2-yl)-2,5-diphenyltetrazolium bromide) (5 mg/mL in H_2O) was added to cells in fresh medium and left for 2 h at 37 °C. The medium was aspirated, 100 μL of DMSO was added to the wells, and color development was measured at 570 nm with an Infinite 200 auto microplate reader (Infinite 200, Tecan, Austria). The absorbance is proportional to the number of viable cells. All measurements were performed in quadruplicate and repeated at least three times. Results are shown as percent of cell viability in comparison with non-treated control cells. Evaluation of statistical significance of differences was performed using Graph Pad INSTAT software (GraphPad software, San Diego, CA, USA). Comparison between groups was assessed by one–way analysis of variance (One–way ANOVA) followed by the Bonferroni Multiple Comparisons Test.

2.4. Hemolytic assays

These assays were done as previously described [40]. Briefly, hemolytic activity was performed by mixing different amounts of cubosomes in Veronal buffer with 50 μL of 10% human erythrocytes (EA) suspended in a final volume of 250 μL. After incubation at 37 °C for 30 min, red cell lysis was calculated by measuring the OD415. Hemolytic activity was expressed as a percentage of lysis ± SD.

2.5. Animal model and treatment

Pathogen-free female BALB/c mice (4- to 6-weeks old) were purchased from Harlan Laboratories (San Pietro al Natisone, Italy). Mice were housed in a controlled environment and maintained with *ad libitum* food and water. Mice were treated intravenously (i.v.) with 150 µL of cubosomes solution, corresponding to ~0.4 nmol Cy5.5-C_{14} and 50 µg MO. Mice were followed by optical imaging images acquisition over time to evaluate the probe biodistribution and accumulation in specific organs. Animals were also subjected to blood samples for plasma collection.

2.6. In vivo and ex vivo time domain optical imaging analysis

Experimental animals were anesthetized with isoflurane at 1.8 - 2.0 volume %, shaved in the abdomen to avoid laser scattering caused by fur, placed in the small animal time-domain Optix MX2 preclinical NIRF-imager (Advanced Research Technologies, Montreal, CA) and maintained under vaporized isoflurane for the entire imaging session. Two-dimensional regions of interest were selected and laser power, integration time and scan step size were optimized according to the emitted signal. A blank image was acquired before i.v. administration of cubosomes to record background signal intensity. After i.v. treatment the animals were monitored at multiple time points. In all imaging experiments, a 670 nm pulsed laser diode with a repetition frequency of 80 MHz and a time resolution of 12 ps light pulse was used for excitation. Fluorescence emission was collected at 700 nm and optical imaging results were analysed by reporting fluorescence intensity values in normalized counts (NC), representing the photon count for unit excitation laser power and unit exposure time, allowing comparison among different images. The fluorescence lifetime results were obtained by fitting every fluorescence decay curve corresponding to each pixel measured by Optix using the Levenberg Marquet least squares method [41]. For *ex vivo* imaging, the last *in vivo* whole body imaging session was followed by euthanasia of animals. Explanted organs were collected,

washed in PBS and analysed with the same Optix system. Following, explanted organs were snap-frozen in isopentane and dry ice and cooled at -80 °C for tissue analysis.

2.7. Ex vivo tissue analyses

For fluorescence microscopy, sections of 7 and 12 μm thickness were cut from frozen organs with a cryostat at -20 °C. Glass slides were kept at 4 °C in the dark and Vectashield Mounting Medium with DAPI (Vector Laboratories, Burlingame, CA), diluted 1:1 with PBS, was used to stain cell nuclei. Fluorescent images were acquired by using an inverted microscope with a CCD camera (DVC-1412AM monochrome digital camera QE > 62% at 550 nm) and the objectives lens 10X, 40X and 63X (NA 1.63) immersion oil.

2.8. Ethical statement

All animal procedures were used to minimize animal pain and suffering. All experimental procedures were performed in strict accordance with the recommendations in the Guide for the Care and Use of the Laboratory Animals of the National Institutes of Health and in compliance with the European (86/609/EEC) and Italian (D.L.116/92) laws. Protocols for mice experimentation were approved by the Institutional Animal Care and Use Committee of the Cluster in Biomedicine (CBM) of the Area Science Park of Trieste and by the Italian Ministry of Health (DM 17/2001-A dd. 02/02/2011).

3. Results and Discussion

To favor its encapsulation within the MO bilayer, a Cyanine 5.5 was modified by adding a long hydrocarbon chain (Cy5.5-C_{14}, see Supplementary Data for details). The fluorescent cubosome formulation was easily prepared by dispersing MO and Cy5.5-

C_{14} in a Pluronic F108 (PF108) aqueous solution. Physicochemical characterization of the formulation was performed by dynamic light scattering (DLS), electron transmission microscopy at cryogenic temperature (cryo-TEM), and small-angle x-ray scattering (SAXS). According to DLS results, the formulation was a homogenous dispersion (polydispersity index of 0.12) of nanoparticles characterized by a mean diameter of 144 ± 1 nm (see figure S1) and a ζ-potential of –21 mV. Nanoparticles morphology, as seen by cryo-TEM, revealed the co-existence of cubic shaped and quasi-spherical objects both displaying an inner structure made of a dark matrix and alternate bright spots (figure 1a), as usually observed in bicontinuous cubic liquid crystalline nanoparticles (cubosomes). The nature of the liquid crystalline phase was assessed by SAXS. The diffraction pattern was characterized by at least five Bragg peaks with relative positions √2:√3:2:√6:√8 (figure 1b), confirming that the inner nanostructure was made of a bicontinuous cubic double diamond phase (space group *Pn3m*), having a lattice parameter of 89.1 ± 0.4 Å. Such a value is about ten percent smaller than that recorded in pristine cubosomes (not containing the fluorescent probe) obtained using the same components [21]. This fact implicitly indicates that, although the nanostructure is retained, accommodation of Cy5.5-C_{14} within the lipid bilayer alters the MO effective packing parameter [42], inducing a slightly higher curvature at the MO/water interface, and a consequent decrease in the lattice parameter.

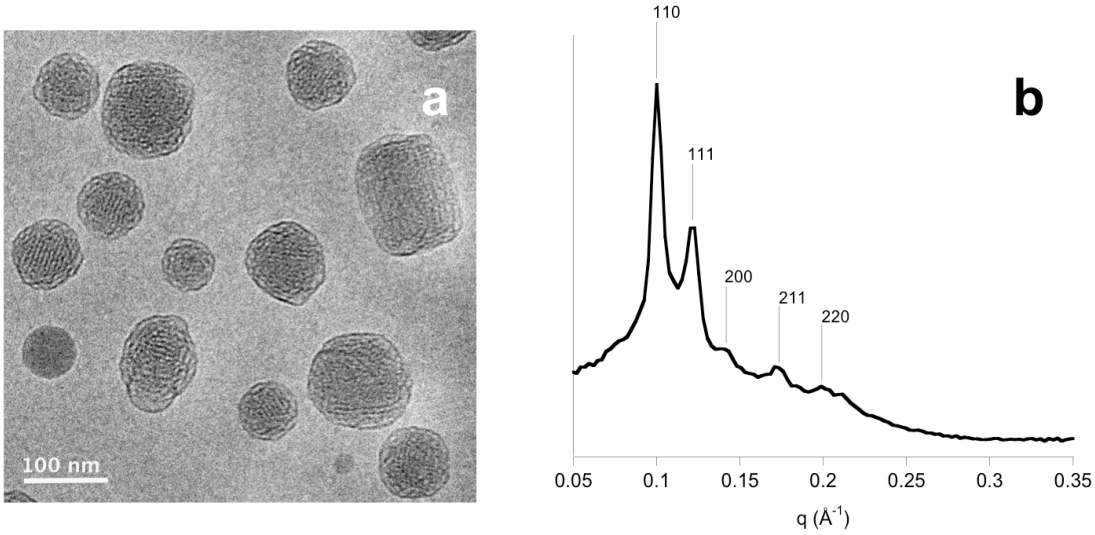

Figure 1. a) *Cryo-TEM image and* ***b)*** *SAXS pattern at 25 °C (Miller indices are also shown on the top of the corresponding Bragg peak) of the cubosome formulation loaded with the Cy5.5-C_{14} dye.*

Photophysical characterization of the dye and the cubosome formulation was performed by UV-Vis and fluorescence spectroscopy. As shown in figure S2 and reported in Table S1, the free dye Cy5.5-C_{14} showed, in EtOH, an absorption band centered at 685 nm (ε = 140000 M^{-1} cm^{-1}) with a shoulder at 650 nm (ε = 14000 M^{-1} cm^{-1}). A strong emission at 709 nm was observed (Φ = 0.27). Once encapsulated inside the cubosomes (Cy5.5-C_{14}@cubosomes, aqueous dispersion), both the absorption (λ_{abs} = 696 nm and 665 nm) and the emission bands (λ_{emis} = 719 nm) of the dye were slightly red-shifted (figure S3), probably due to the more apolar environment experienced by the fluorophore inside the nanoparticles with respect to EtOH. Moreover, a significant difference was recorded between the r value of the free dye and the encapsulated dye (r = 0.008 and r = 0.100 for Cy5.5-C_{14} and Cy5.5-C_{14}@cubosomes, respectively). This difference is caused by the

reduced mobility of the fluorophore inside the nanoparticles, and gives another proof of the internalization of the Cy5.5-C_{14} inside the cubosome formulation.

Before the evaluation *in vivo* as diagnostic tool, the formulation was tested *in vitro* for its toxicity. Indeed, several recent *in vitro* investigations drew attention to the potential cytotoxicity of cubosomes and, particularly, to their hemolytic properties [43,44]. Remarkably, there are some evidences that stabilization of these kind of nanoparticles by means of lipid-PEG conjugates may reduce their cytotoxicity [23,45]. Accordingly, the proposed formulation was investigated for its cytotoxicity against 3T3 cells and erythrocytes. Several experiments reported in the literature evidenced that the cytotoxicity of cubosomes strongly depends on the cellular line investigated. However, the minimum dose reported of monoolein-based cubosomes necessary to induce cytotoxicity is around 20 µg/mL of MO [10,46–48]. The formulation here tested was found to induce no cytotoxicity in 3T3 cells up to 55 µg/mL of MO (figure 2a).

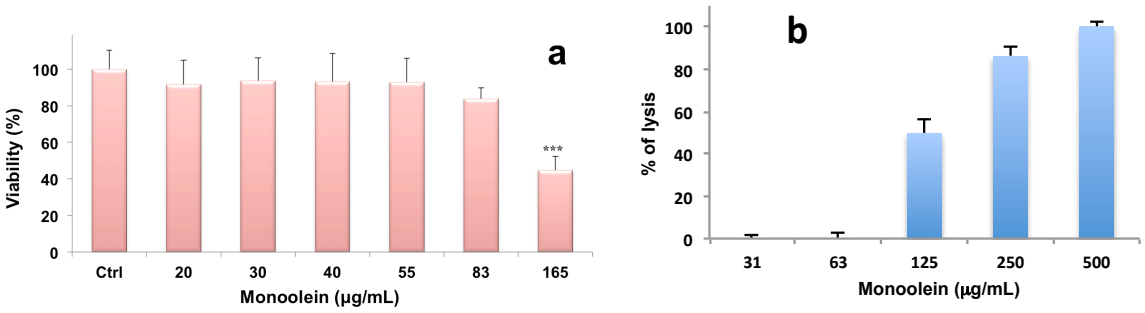

Figure 2. *(**a**) Viability, expressed as % of the control, induced by incubation for 4 h with different concentrations of cubosomes (corresponding to 20-165 µg/mL of MO) in 3T3 fibroblasts by MTT assay. Data are expressed as a mean ± standard deviation (SD) of three independent experiments involving quadruplicate analyses for each sample;* *** *= $p < 0.001$ versus Ctrl. (**b**) Hemolysis test of human red blood cells incubated with different amounts of cubosomes in a standard hemolytic assay using 10% erythrocytes. Data were expressed as % of lysis ± SD.*

Modifying a standard hemolytic assay [49] and using 10^9 erythrocytes (figure 2b) [50,51], incubation of Cy5.5-C_{14}@cubosomes with human red blood cells evidenced the capacity of inducing direct lysis of erythrocytes in a dose-dependent manner. These results are in line with experiments previously reported [48,52], and evidenced that the cubosomes formulation here proposed did not provoke ~~show~~ lysis of erythrocytes below 62 µg/mL of monoolein.

Consequently, *in vivo* experiments were performed using a MO concentration of about 50 µg per mL of plasma. After *in vivo* injection of Cy5.5-C_{14}@cubosomes into the tail vein (i.v.) of a healthy mouse, distribution of the fluorophore was monitored using TD-OI. This technology was useful in understanding the lifetime distribution, and provided a convenient route of analyzing the biodistribution and plasmatic elimination of a fluorescent cubosomes formulation after intravenous administration in mice. Optical imaging was performed two times during the first day, then every 24 hours for the next two days: results showed that, following injection, Cy5.5-C_{14}@cubosomes were rapidly taken up by the liver (figure 3a).

To further investigate the extent of Cy5.5-C_{14}@cubosomes and/or free dye accumulation in the organs and tissues, mice were sacrificed 48 hours after injection of cubosomes for *ex vivo* TD-OI analysis of explanted organs (i.e., kidneys, thymus, heart, spleen, brain, lungs, stomach, intestine, and liver). This approach excludes any potential influence due to autofluorescence and scattering within the body and fur, thereby increasing both specificity and sensitivity of the probe detection. *Ex vivo* evaluation of organs 48 hours post-injection showed that the highest fluorescence intensity was localized in the liver and stomach, emphasizing that Cy5.5-C_{14} is excreted through these organs (figure 3b).

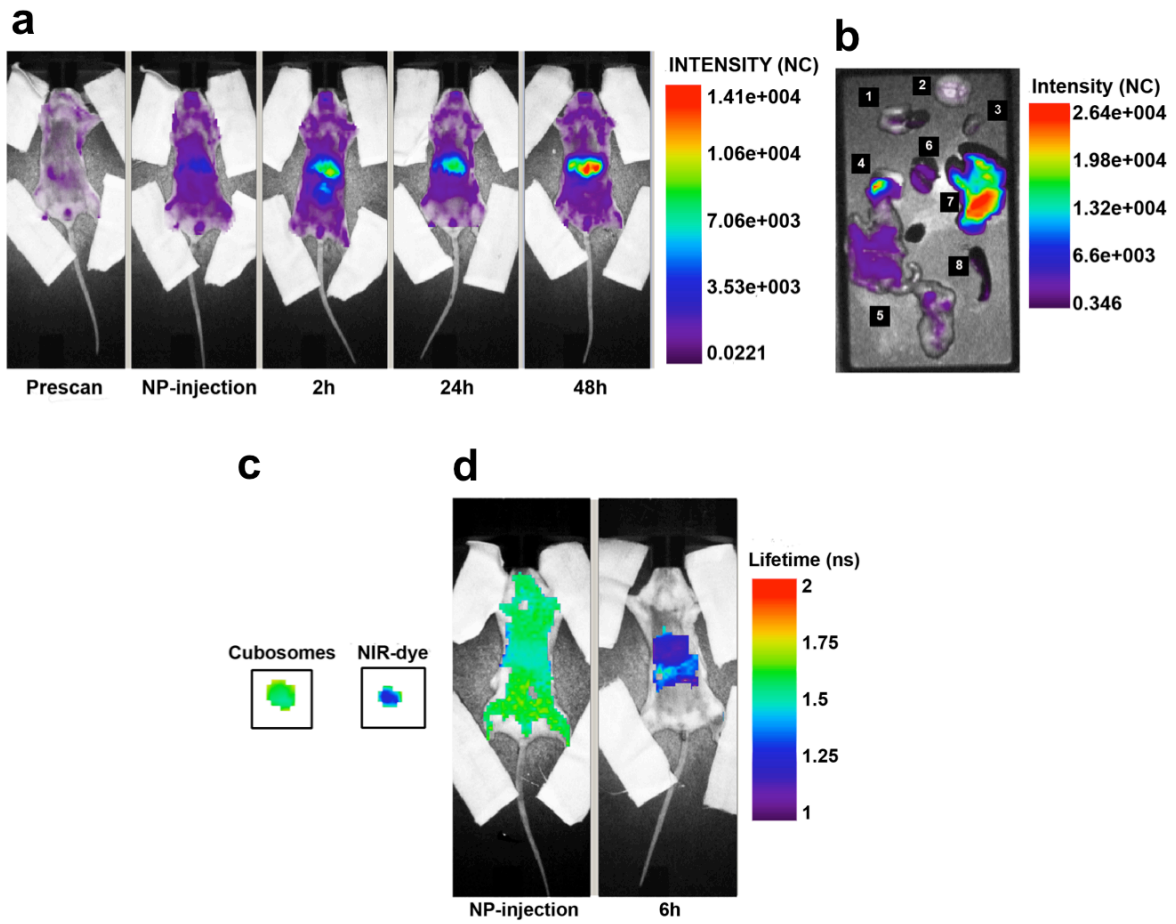

Figure 3. *(**a**) Whole body fluorescence intensity distribution of a representative healthy mouse that received an i.v. injection of cubosomes (150 μL, corresponding to ~0.4 nmol Cy5.5-C_{14} and 50 μg MO, see the text), displayed in normalized counts (NC). Following injection, cubosomes were rapidly taken up by the liver. (**b**) In accordance to in vivo results, ex vivo analysis clearly showed that the highest signal of fluorescence emission was associated with liver. 1. Lungs and heart; 2. Brain; 3. Thymus; 4. Stomach; 5. Intestine; 6. Kidney; 7. Liver; 8. Spleen. (**c**) In vitro fluorescence lifetime analysis with equimolar aliquots of the cubosome formulation and the control NIR-dye. Samples were placed on a paper substrate before analysis of the lifetime. Fluorescence lifetime maps were created from temporal point-spread function (TPSF) data acquired using the TD-FOI imaging system. (**d**) Representative in vivo fluorescence lifetime maps of whole body mice injected with cubosomes. Images were taken few minutes and 6 hours after the injection.*

Fluorescence lifetime information is complementary to intensity measurement and can be used to improve signal-to-background contrast and provide environment-sensing capability. Some biological events not available from fluorescent intensity images can be monitored directly from the fluorescence lifetime map. Fluorescence decays of Cy5.5-C_{14}@cubosomes and Cy5.5-C_{14} were measured *in vitro* and single-exponential models were appropriately fitted. Cy5.5-C_{14} clearly changed its fluorescence lifetime properties once loaded in the cubosomes formulation (figure 3c).

This provided the possibility to discriminate *in vivo* between the Cy5.5-C_{14}@cubosomes and the free dye based on distinct lifetime profiles. Whole body imaging analysis few minutes after i.v. injection revealed a diffuse distribution of cubosomes throughout the body of the mouse and, after the first 6 hours, a strong signal, decreasing over time and associated with the free dye, was clearly detectable mainly in the liver and intestine, (figure 3d).

Cy5.5-C_{14}@cubosome plasmatic elimination after single i.v. administration was investigated by analyzing the fluorescence signal of plasma samples at different times post-injection.~~,~~ An exponential time decay of the average intensity suggested an underlying first-order kinetic (figure S4). Circulating profile of the nanoparticles obtained from these experiments evidenced a half-life of approximately 2 hours. This result is in good agreement with that reported on similar MO-based nanoparticles radiolabelled with a tracer molecule [12].

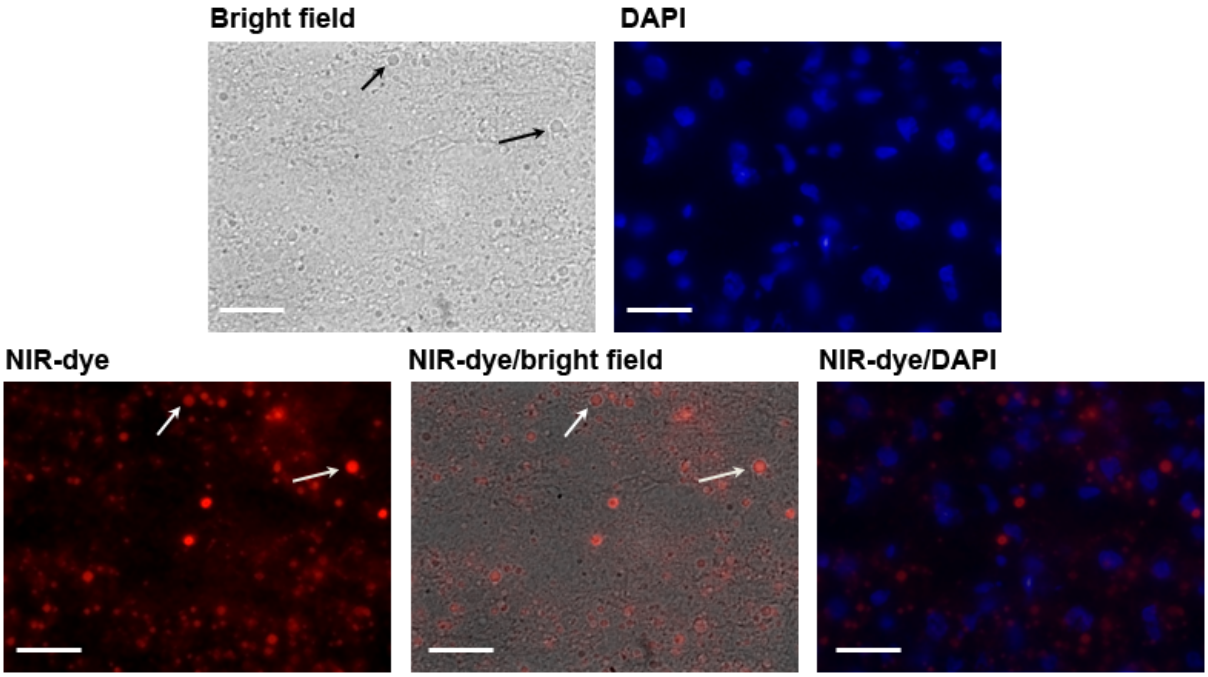

Figure 4. *Representative microscopy images of cryo-sections obtained from liver explanted from the cubosomes injected mice. Sections are imaged under bright field and fluorescence mode under x63. DAPI staining was carried out to visualize cell nuclei, which appear in blue, while Cy5.5-C_{14} appears in red. The arrows indicate droplet structures in the hepatic parenchyma (bar = 15 μm).*

To cross-validate the results obtained *in vivo* and *ex vivo*, localization of Cy5.5-C_{14} within the liver was confirmed by fluorescence microscopy examination of tissue cryo-sections obtained from the explanted organ 48 hours after Cy5.5-C_{14}@cubosomes injection (figure 4). Close examination of the liver cryo-sections revealed the presence of several spherical fluorescent aggregates (indicated by the arrows) with size in the micrometer range, which could reasonably be identified as the lipid droplets (cytoplasmic organelles involved in neutral lipid storage). It deserves here noticing that MO-based nanoparticles (cubosomes, or vesicles) are readily internalized after exposure to cells, causing growth in size and number of the lipid droplets [21,46,53]. Moreover, given the high hydrophobic nature of Cy5.5-C_{14}, following the

nanoparticle disassembling after cellular internalization, the released dye should preferentially stain structures of this kind in the cells.

4. Conclusions

Cubosomes belong to a special class of nanoparticles characterized by the liquid crystalline nature of their nanostructure, and numerous recently published papers demonstrated their potential as diagnostic/theranostic tools. Here, an innovative cubosomes formulation loaded with a NIR-emitting imaging dye to confer these nanoparticles fluorescent properties useful for *in vivo* TD-FOI applications was investigated. Physicochemical analysis performed by SAXS confirmed the reverse cubic bicontinuous structure of the nanoparticles, and photophysical analysis proved the fluorescence profile of the dye is retained after its encapsulation within the cubosomes, with a substantial increase of the fluorescence lifetime. After intravenous administration at a non-cytotoxic concentration, TD-FOI analysis evidenced the diffuse distribution of the cubosomes throughout the whole body of the mouse and their intestinal and hepatic elimination with a -first order kinetic. Finally, we showed the lifetime contrast could be used to distinguish cubosomes fluorescence from free dye fluorescence and from background nonspecific signal.

Because of its high sensitivity, FOI has been increasingly applied in assessing tissue pathology, as in image-guided surgery, and for sentinel lymph node fluorescence mapping. In this respect, several intraoperative NIR fluorescence systems are now available for pre-clinical and clinical studies and some of them have been approved by the FDA for use in humans [54]. In addition, fluorescence lifetime imaging is a powerful tool ~~to~~ in investigating the molecules microenvironment, and has been widely used in modern microscopy. A combination of environmental sensitivity and chemical properties renders fluorescence lifetime as a separate yet complementary approach to conventional fluorescence intensity analysis. However, despite

its significant impact in the context of microscopy, fluorescence lifetime imaging *in vivo* for applications in medical research has been delayed until the availability of a commercial time-domain imager.

From a molecular imaging perspective, it was here noted that cubosomes have great applicative potential in medicine as fluorescence and lifetime probes. For this purpose, more progresses of fluorescent cubosomes towards *in vivo* applications will depend on the introduction of targeting properties that will increase the specificity of the cubosomes to be used for both imaging and therapeutic applications.

Acknowledgements

Fondazione Banco di Sardegna and Regione Autonoma della Sardegna (CRP-59699) are gratefully acknowledged. The cryo-TEM work was performed at the Technion Laboratory for Electron Microscopy of Soft Matter, supported by the Technion Russell Berrie Nanotechnology Institute (RBNI).

References

[1] Hyde S T 1996 Bicontinuous structures in lyotropic liquid crystals and crystalline hyperbolic surfaces *Curr. Opin. Solid State Mater. Sci.* **1** 653–62

[2] Hyde S, Ninham B W, Andersson S, Larsson K, Landh T, Blum Z and Lidin S 1997 *The Language of Shape* (Elsevier)

[3] Larsson K 1983 Two cubic phases in monoolein water system *Nature* **304** 664

[4] Mulet X, Boyd B J and Drummond C J 2013 Advances in drug delivery and medical imaging using colloidal lyotropic liquid crystalline dispersions *J. Colloid Interface Sci.* **393** 1–20

[5] Demurtas D, Guichard P, Martiel I, Mezzenga R, Hebert C and Sagalowicz L 2015

Direct visualization of dispersed lipid bicontinuous cubic phases by cryo-electron tomography. *Nat. Commun.* **6** 8915

[6] Gustafsson J, Ljusberg-wahren H and Almgren M 1996 Cubic Lipid-Water Phase Dispersed into Submicron Particles *Langmuir* **12** 4611–3

[7] Landh T 1994 Phase Behavior in the System Pine Oil Monoglycerides-Poloxamer 407-Water at 20 °C *J. Phys. Chem.* **98** 8453–67

[8] Azmi I D, Moghimi S M and Yaghmur A 2015 Cubosomes and hexosomes as versatile platforms for drug delivery *Ther. Deliv.* **6** 1347–64

[9] Meli V, Caltagirone C, Falchi A M, Hyde S T, Lippolis V, Monduzzi M, Obiols-Rabasa M, Rosa A, Schmidt J, Talmon Y and Murgia S 2015 Docetaxel-Loaded Fluorescent Liquid-Crystalline Nanoparticles for Cancer Theranostics *Langmuir* **31** 9566–75

[10] Deshpande S, Venugopal E, Ramagiri S, Bellare J R, Kumaraswamy G and Singh N 2014 Enhancing cubosome functionality by coating with a single layer of poly-ε-lysine. *ACS Appl. Mater. Interfaces* **6** 17126–33

[11] Murgia S, Falchi A M, Meli V, Schillén K, Lippolis V, Monduzzi M, Rosa A, Schmidt J, Talmon Y, Bizzarri R and Caltagirone C 2015 Cubosome formulations stabilized by a dansyl-conjugated block copolymer for possible nanomedicine applications *Colloids Surfaces B* **129** 87–94

[12] Muir B W, Acharya D P, Kennedy D F, Mulet X, Evans R A, Pereira S M, Wark K L, Boyd B J, Nguyen T-H, Hinton T M, Waddington L J, Kirby N, Wright D K, Wang H X, Egan G F and Moffat B A 2012 Metal-free and MRI visible theranostic lyotropic liquid crystal nitroxide-based nanoparticles *Biomaterials* **33** 2723–33

[13] Boge L, Bysell H, Ringstad L, Wennman D, Umerska A, Cassisa V, Eriksson J, Joly-Guillou M-L, Edwards K and Andersson M 2016 Lipid-Based Liquid Crystals As

Carriers for Antimicrobial Peptides: Phase Behavior and Antimicrobial Effect. *Langmuir* **32** 4217–28

[14] Kim H and Leal C 2015 Cuboplexes : Topologically Active siRNA Delivery *ACS Nano* **9** 10214–26

[15] Chong J Y T, Mulet X, Postma A, Keddie D J, Waddington L J, Boyd B J and Drummond C J 2014 Novel RAFT amphiphilic brush copolymer steric stabilisers for cubosomes: poly(octadecyl acrylate)-block-poly(polyethylene glycol methyl ether acrylate). *Soft Matter* **10** 6666–76

[16] Chong J Y T, Mulet X, Waddington L J, Boyd B J and Drummond C J 2011 Steric stabilisation of self-assembled cubic lyotropic liquid crystalline nanoparticles: high throughput evaluation of triblock polyethylene oxide-polypropylene oxide-polyethylene oxide copolymers *Soft Matter* **7** 4768

[17] Chong J Y T, Mulet X, Waddington L J, Boyd B J and Drummond C J 2012 High-throughput discovery of novel steric stabilizers for cubic lyotropic liquid crystal nanoparticle dispersions *Langmuir* **28** 9223–32

[18] Johnsson M, Barauskas J, Norlin A and Tiberg F 2006 Physicochemical and Drug Delivery Aspects of Lipid-Based Liquid Crystalline Nanoparticles: A Case Study of Intravenously Administered Propofol *J. Nanosci. Nanotechnol.* **6** 3017–24

[19] Barreto J A, O'Malley W, Kubeil M, Graham B, Stephan H and Spiccia L 2011 Nanomaterials: Applications in Cancer Imaging and Therapy *Adv. Mater.* **23** H18–40

[20] García K P, Zarschler K, Barbaro L, Barreto J A, O'Malley W, Spiccia L, Stephan H and Graham B 2014 Zwitterionic-Coated "Stealth" Nanoparticles for Biomedical Applications: Recent Advances in Countering Biomolecular Corona Formation and Uptake by the Mononuclear Phagocyte System *Small* **10** 2516–29

[21] Caltagirone C, Falchi A M, Lampis S, Lippolis V, Meli V, Monduzzi M, Prodi L,

Schmidt J, Sgarzi M, Talmon Y, Bizzarri R and Murgia S 2014 Cancer-cell-targeted theranostic cubosomes. *Langmuir* **30** 6228–36

[22] Zhai J, Scoble J A, Li N, Lovrecz G, Waddington L J, Tran N, Muir B W, Coia G, Kirby N, Drummond C J and Mulet X 2015 Epidermal growth factor receptor-targeted lipid nanoparticles retain self-assembled nanostructures and provide high specificity *Nanoscale* **7** 2905–13

[23] Jain V, Swarnakar N K, Mishra P R, Verma A, Kaul A, Mishra A K and Jain N K 2012 Paclitaxel loaded PEGylated gleceryl monooleate based nanoparticulate carriers in chemotherapy *Biomaterials* **33** 7206–20

[24] Nilsson C, Barrios-Lopez B, Kallinen A, Laurinmäki P, Butcher S J, Raki M, Weisell J, Bergström K, Larsen S W, Østergaard J, Larsen C, Urtti A, Airaksinen A J and Yaghmur A 2013 SPECT/CT imaging of radiolabeled cubosomes and hexosomes forpotential theranostic applications *Biomaterials* **34** 8491–503

[25] Bye N, Hutt O E, Hinton T M, Acharya D P, Waddington L J, Mo B A, Wright D K, Wang H X, Mulet X and Muir B W 2014 Nitroxide-Loaded Hexosomes Provide MRI Contrast in Vivo *Langmuir* **30**8898−8906

[26] Li X, Gao X, Shi W and Ma H 2014 Design strategies for water-soluble small molecular chromogenic and fluorogenic probes *Chem. Rev.* **114** 590–659

[27] Luo S, Zhang E, Su Y, Cheng T and Shi C 2011 A review of NIR dyes in cancer targeting and imaging *Biomaterials* **32** 7127–38

[28] Schätzel K 1991 Suppression of Multiple Scattering by Photon Cross-correlation Techniques *J. Mod. Opt.* **38** 1849–65

[29] Umezawa K, Citterio D and Suzuki K 2014 New trends in near-infrared fluorophores for bioimaging. *Anal. Sci.* **30** 327–49

[30] Gabbani T, Manetti N, Bonanomi A G, Annese A L and Annese V 2015 New

endoscopic imaging techniques in surveillance of inflammatory bowel disease. *World J. Gastrointest. Endosc.* **7** 230–6

[31] Agostinis C, Biffi S, Garrovo C, Durigutto P, Lorenzon A, Bek A, Bulla R, Grossi C, Borghi M O, Meroni P and Tedesco F 2011 In vivo distribution of β2 glycoprotein I under various pathophysiologic conditions. *Blood* **118** 4231–8

[32] Berenzin M Y, Lee H, Akers W, Guo K, Goiffon R J, Almutairi A, Fréchet J M and Achilefu S 2009 No Title *Conf. Proc. IEEE Eng. Med. Biol. Soc.* 114

[33] Biffi S, Garrovo C, Macor P, Tripodo C, Zorzet S, Secco E, Tedesco F and Lorusso V 2008 In vivo biodistribution and lifetime analysis of Cy5.5-conjugated rituximab in mice bearing lymphoid tumor xenograft using time-domain near-infrared optical imaging *Mol. Imaging* **7** 272–82

[34] Biffi S, Petrizza L, Rampazzo E, Voltan R, Sgarzi M, Garrovo C, Prodi L, Andolfi L, Agnoletto C, Zauli G and Secchiero P 2014 Multiple dye-doped NIR-emitting silica nanoparticles for both flow cytometry and in vivo imaging *RSC Adv.* **4** 18278

[35] Garrovo C, Bergamin N, Bates D, Cesselli D, Beltrami A P, Lorenzon A, Ferrari R, Alberto Beltrami C, Lorusso V and Biffi S 2013 In vivo tracking of murine adipose tissue-derived multipotent adult stem cells and ex vivo cross-validation. *Int. J. Mol. Imaging* **2013**

[36] Inagawa K, Oohashi T, Nishida K, Minaguchi J, Tsubakishita T, Yaykasli K O, Ohtsuka A, Ozaki T, Moriguchi T and Ninomiya Y 2009 Optical imaging of mouse articular cartilage using the glycosaminoglycans binding property of fluorescent-labeled octaarginine *Osteoarthr. Cartil.* **17** 1209–18

[37] Rurack K and Spieles M 2011 Fluorescence quantum yields of a series of red and near-infrared dyes emitting at 600-1000 nm *Anal. Chem.* **83** 1232–42

[38] Montalti M, Credi C, Prodi L and Gandolfi M T 2006 *Handbook of Photochemistry*

(Boca Raton: CRC Press, Taylor and Francis Group)

[39] Rosa A, Murgia S, Putzu D, Meli V and Falchi A M 2015 Monoolein-based cubosomes affect lipid profile in HeLa cells *Chem. Phys. Lipids* **191** 96–105

[40] Marzari R, Sblattero D, Macor P, Fischetti F, Gennaro R, Marks J D, Bradbury A and Tedesco F 2002 The cleavage site of C5 from man and animals as a common target for neutralizing human monoclonal antibodies: in vitro and in vivo studies. *Eur. J. Immunol.* **32** 2773–82

[41] Abulrob A, Brunette E, Slinn J, Baumann E and Stanimirovic D In vivo time domain optical imaging of renal ischemia-reperfusion injury: discrimination based on fluorescence lifetime *Mol. Imaging* **6** 304–14

[42] Angius R, Murgia S, Berti D, Baglioni P and Monduzzi M 2006 Molecular recognition and controlled release in drug delivery systems based on nanostructured lipid surfactants *J. Phys. Condens. Matter* **18** S2203–20

[43] Barauskas J, Cervin C, Jankunec M, Špandyreva M, Ribokaitė K, Tiberg F and Johnsson M 2010 Interactions of lipid-based liquid crystalline nanoparticles with model and cell membranes *Int. J. Pharm.* **391** 284–91

[44] Bode J C, Kuntsche J, Funari S S and Bunjes H 2013 Interaction of dispersed cubic phases with blood components. *Int. J. Pharm.* **448** 87–95

[45] Zhai J, Hinton T M, Waddington L J, Fong C, Tran N, Mulet X, Drummond C J and Muir B W 2015 Lipid-PEG Conjugates Sterically Stabilize and Reduce the Toxicity of Phytantriol-Based Lyotropic Liquid Crystalline Nanoparticles. *Langmuir* **31** 10871–80

[46] Falchi A M, Rosa A, Atzeri A, Incani A, Lampis S, Meli V, Caltagirone C and Murgia S 2015 Effects of monoolein-based cubosome formulations on lipid droplets and mitochondria of HeLa cells *Toxicol. Res.* **4** 1025–36

[47] Hartnett T E, Ladewig K, O'Connor A J, Hartley P G and McLean K M 2015

Physicochemical and cytotoxicity analysis of glycerol monoolein-based nanoparticles *Rsc Adv.* **5** 26543–9

[48] Tran N, Mulet X, Hawley A M, Hinton T M, Mudie S T, Muir B W, Giakoumatos E C, Waddington L J, Kirby N M and Drummond C J 2015 Nanostructure and cytotoxicity of self-assembled monoolein–capric acid lyotropic liquid crystalline nanoparticles *RSC Adv.* **5** 26785–95

[49] Durigutto P, Macor P, Ziller F, De Maso L, Fischetti F, Marzari R, Sblattero D and Tedesco F 2013 Prevention of arthritis by locally synthesized recombinant antibody neutralizing complement component C5. *PLoS One* **8** e58696

[50] Fridkis-Hareli M, Storek M, Mazsaroff I, Risitano A M, Lundberg A S, Horvath C J and Holers M V. 2011 Design and development of TT30, a novel C3d-targeted C3/C5 convertase inhibitor for treatment of human complement alternative pathway-mediated diseases *Blood* **118** 4705–13

[51] Zhang Y, Shao D, Ricklin D, Hilkin B M, Nester C M, Lambris J D and Smith R J H 2015 Compstatin analog Cp40 inhibits complement dysregulation in vitro in C3 glomerulopathy. *Immunobiology* **220** 993–8

[52] Hinton T M, Grusche F, Acharya D, Shukla R, Bansal V, Waddington L J, Monaghan P and Muir B W 2014 Bicontinuous cubic phase nanoparticle lipid chemistry affects toxicity in cultured cells *Toxicol. Res. (Camb).* **3** 11–22

[53] Carboni M, Falchi A M, Lampis S, Sinico C, Manca M L, Schmidt J, Talmon Y, Murgia S and Monduzzi M 2013 Physicochemical, Cytotoxic, and Dermal Release Features of a Novel Cationic Liposome Nanocarrier *Adv. Healthc. Mater.* **2** 692–701

[54] Mondal S B, Gao S, Zhu N, Liang R, Gruev V and Achilefu S 2014 Real-time Fluorescence Image-Guided Oncologic Surgery *Adv. Cancer Rres.* **124** 171–211